STANDARDIZATION OF Hα PHOTOMETRY USING OPEN CLUSTERS

III. THE PLEIADES

by

Mana Philip Vautier

A senior thesis submitted to the faculty of

Brigham Young University

in partial fulfillment of the requirements for the degree of

Bachelor of Science

Department of Physics and Astronomy

Brigham Young University

April 2006

BRIGHAM YOUNG UNIVERSITY

DEPARTMENT APPROVAL

of a senior thesis submitted by

Mana Philip Vautier

This thesis has been reviewed by the research advisor, research coordinator, and department chair and has been found to be satisfactory.

Date	Michael D. Joner, Advisor
Date	Jean-François Van Huele, Research Coordinator
Date	Scott D. Sommerfeldt, Chair

ABSTRACT

STANDARDIZATION OF Hα PHOTOMETRY USING OPEN CLUSTERS

III. THE PLEIADES

Mana Philip Vautier

Department of Physics and Astronomy

Bachelor of Science

This thesis establishes a standard catalogue for an Hα photometric system based on observation of selected field stars as well as main sequence stars in the nearby open cluster known as the Pleiades. All observations were made through Hα wide (210Å) and narrow (30Å) passbands. Using a color index centered on a single wavelength eliminates effects resulting from atmospheric extinction and produces a reddening-free temperature index. The Hα index also has several advantages over the Hβ index including greater CCD quantum efficiency, less line blanketing and the ability to detect a wider range of spectral types. As part of a bigger project, data from this thesis will be combined with data taken on other clusters to produce a master catalogue. All data were collected from Brigham Young University's Orson Pratt and West Mountain observatories.

ACKNOWLEDGMENTS

I would like to acknowledge all my professors who helped me get to where I am today. I am especially grateful to my advisor, Professor Michael Joner for allowing me to work along side him with his research, and for his continual guidance throughout the project. Not to mention the fact that he has the best collection of manned space flight memorabilia I have ever seen. I am also grateful to Dr. Benjamin Taylor for always being so willing to answer any questions, and especially for offering his statistical expertise. He was also the one to introduce me to the wonderful world of Feghoots. I would be amiss if I did not acknowledge Canon Laverty, a true friend indeed with whom I shared this project, for all the fun (and tiring) times we had together. I also want to acknowledge my parents who instilled in me a belief that I could do anything I truly put my mind to. Finally, I want to express my love and appreciation to my wife Annette for her continual love and support. She, along with our son Michael, always helped me to remember what is most important in life, and where my priorities lie.

Contents

List of Figures

List of Tables

Chapter 1

Introduction

1.1 Motivation

If interstellar transportation were possible, it would be very easy to measure intrinsic values of stellar properties through direct measurements. Knowing stellar properties helps us better understand stellar life cycles, which lead to a greater understanding of the universe in which we live. Temperature in particular is a fundamental property of a star, as it allows us to derive other useful information about the star such as luminosity, apparent and absolute magnitudes, spectral types, approximate age, and distance. Unfortunately, long distance space travel is not yet possible, so we must rely on alternative methods to obtain our measurements.

Many of these methods do not produce reliable results due to errors caused by atmospheric extinction and interstellar reddening. The method used here is not sensitive to many of the errors incurred through other methods, and therefore yields significantly more accurate data. This research establishes a reliable catalogue of Hα indices in the Pleiades (Fig. 1.1) cluster. This cluster is ideal to use for several reasons. First, it is relatively close. Second, it has been studied previously by many

people using many different techniques. Third, it contains many stars spanning a wide variety of temperatures along the main sequence. This research is also part of a bigger project. Data taken on several other clusters including NGC 752, Praesepe, Coma and the Hyades, as well as 30 field stars, will be combined with data from this project to produce a master catalogue of Hα indices. This catalogue will then be made available for more precise calibrations on future projects.

Figure 1.1: Portion of the young open cluster Pleiades. (West Mountain Observatory)

1.2 Color Index

There are many different ways to characterize a star. This research focuses on the property of temperature, which can be obtained using two primary techniques. One method uses high resolution spectroscopy and comparison with standard spectra. Obtaining these spectra, however, can be very difficult and time consuming. The other, easier method utilizes the "color" of a star, which is directly related to its temperature.

A star's color, or color index, is a numerical value commonly obtained by measuring the magnitude (Sec. 2.4) of an object through two filters centered on different wavelengths. The index is the difference between these two measured magnitudes. Since the intensity of light given off by a star at any given wavelength is dependent upon the temperature of the star (Fig. 2.4), comparing the brightness in these two filters yields the temperature. Current detectors are able to measure magnitudes across much of the electromagnetic spectrum, so there is a wide variety of magnitude systems available to choose from. Two commonly used systems are the Johnson-Cousins UBVRI system [1] [2], and the Strömgren *uvby* system [3] . An illustration of the two different effective wavelengths used to obtain a Strömgren *b-y* color index is shown in Fig. 1.2.

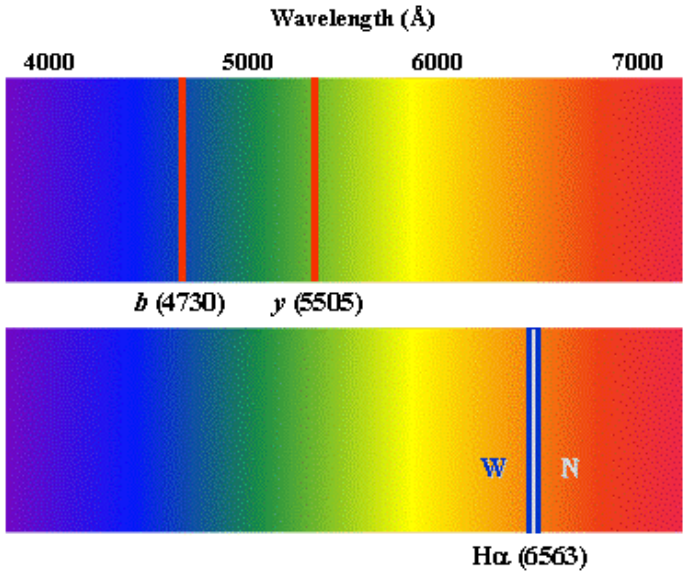

Figure 1.2: Top: Strömgren b and y filters centered on two different wavelengths. Bottom: Hα filters are centered on the same wavelength (6563Å).

Sometimes an index may be obtained by measuring the magnitude of an object through two filters centered on the same wavelength. To do this the filters must have different bandwidths , one wide and the other narrow. This research utilizes a set of hydrogen filters centered on a wavelength of 6563Å (Fig. 1.2), corresponding to the Hα absorption line of the Balmer series. More details on these filters will be given in Sec. 2.3.

1.3 The Hα Absorption Line

To better understand the origin of the Hα line, a brief background of atomic theory is given. In 1911, Sir Ernest Rutherford of New Zealand first proposed the nuclear model of the atom. After spending a year working with him, Niels Bohr presented two postulates concerning atomic theory. His first postulate stated that *only a discrete number of orbits are allowed to the electron and when in those orbits, the electron cannot radiate* [4]. Each quantized orbit is assigned a principal quantum number n, where $n = 1$ represents the lowest orbit, called the ground state. There is also a specific energy difference between orbitals given by

$$\Delta E(\lambda) = \frac{hc}{\lambda} \tag{1.1}$$

where $h = 6.623 \times 10^{-34}$ J·s is Planck's constant, $c = 3 \times 10^{8}$ m/s is the speed of light and λ is the wavelength of light either emitted or absorbed.

Bohr's second postulate explained the conditions under which an electron can radiate by stating that (a) *radiation in the form of a single discrete quantum is emitted or absorbed as the electron jumps from one orbit to another*, and (b) *the energy of this radiation equals the energy difference between the orbits* [4]. When an atom absorbs a photon of exactly the right energy, an electron can make a transition

from a lower orbit to a higher one. The greater the energy of the photon, the larger the transition. This process produces absorption lines which are observed as dark lines on a continuous spectrum as shown in Fig. 1.3.

Although transitions can take place between any two orbitals, only those that start or finish at the first excited state $n = 2$ appear in the visible spectrum. These special transitions are denoted as Balmer series transitions. Since Eq. 1.1 shows that energy is inversely proportional to wavelength, a high energy photon produces a dark line at a smaller wavelength than a low energy photon. For the Balmer series, this means that a transition to the $n = 3$ state will produce an absorption line in the red region, whereas a transition to the $n = 4$ state will produce an absorption line in the blue region. These lines are designated Hα and Hβ respectively, and the exact wavelength λ at which the absorption lines form can be found using Eq. 1.2 where $R = 1.096776 \times 10^7$ m^{-1} is the Rydberg constant and the subscripts a and b represent the initial and final energy levels.

$$\frac{1}{\lambda_{ab}} = R(\frac{1}{n_b^2} - \frac{1}{n_a^2}) \tag{1.2}$$

The strength of an absorption line is directly related to the temperature of the star. Fig. 1.3 illustrates how absorption lines for hydrogen are strongest in early A-type stars, which have an approximate surface temperature of 10,000 Kelvin (K). Stars at this temperature cause the greatest number of Balmer transitions which result in especially strong, dark Hydrogen absorption lines. Cooler stars, however, excite fewer electrons, meaning that less light is being absorbed. Consequently, more light at these wavelengths reaches us on the earth and the absorption lines gradually disappear.

As the star's temperature increases, the absorption lines also become weaker, but

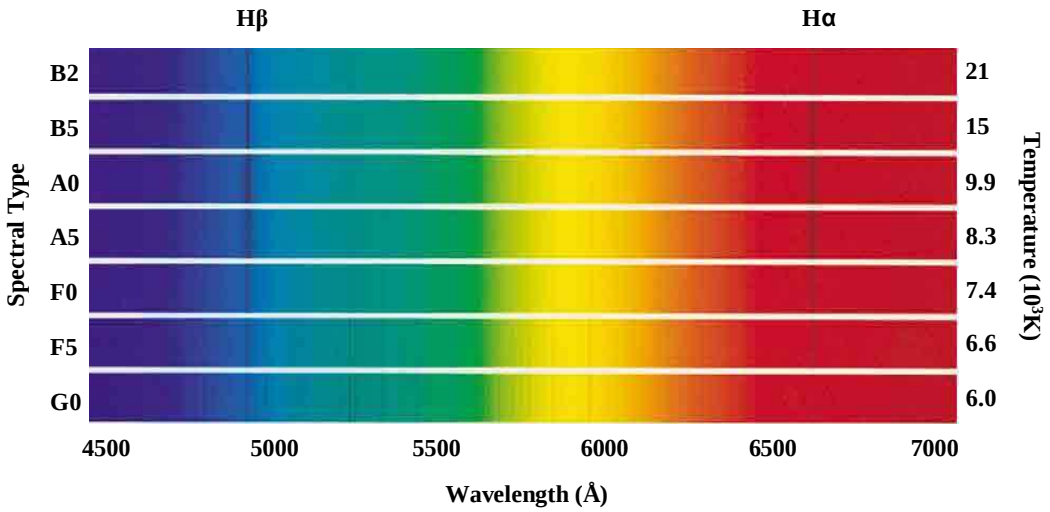

Figure 1.3: Spectrum showing the strength of the Hα and Hβ absorption lines for different spectral types. Adapted from http://spot.pcc.edu/∼aodman/physics%20122/luminosity%20pictures/luminosity%20lecture.htm

not for the same reason. Ionization of hydrogen begins above 10,000 K. This means that the electrons in the hydrogen atom absorb so much energy that they break free of the atom altogether, and without electrons, transitions cannot take place. So for hotter stars, the number of ionized atoms increases and once again the absorption lines gradually disappear.

As can be seen from Fig. 1.4, the narrow filter for this project is centered very tightly on the Hα absorption line, and therefore transmits a very narrow range of wavelengths. The wide filter, however, transmits wavelengths up to 210Å on either side of the absorption line. This means that the wide filter effectively measures the continuum, while the narrow filter measures the strength, or depth, of the absorption line. A difference in magnitudes obtained through these two filters is known as a Narrow-minus-Wide color index (N-W).

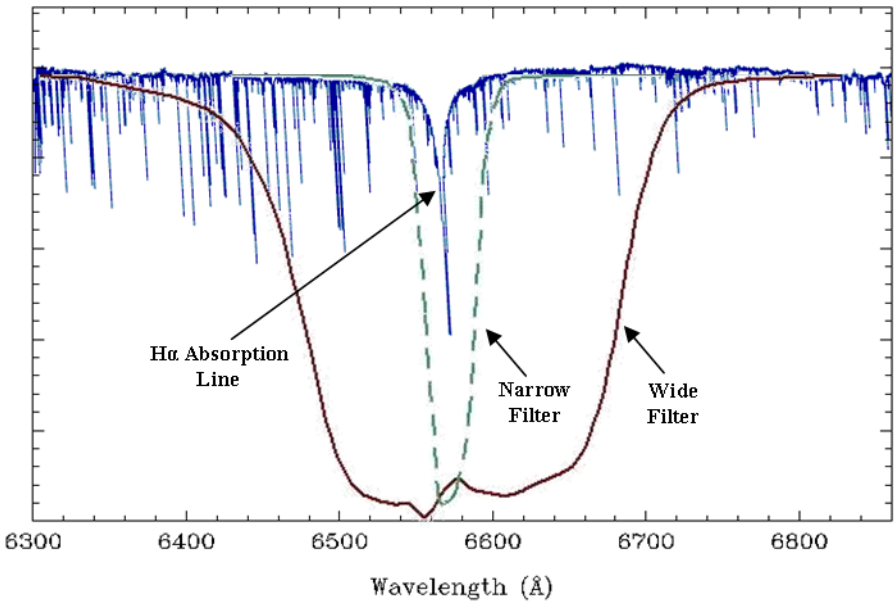

Figure 1.4: Transmission curves of the Hα wide and narrow filters laid over the Hα absorption line from a typical F5IV star.

1.4 Advantages of a Single Wavelength Index

The interstellar medium (ISM) is pervaded by particles, gas, dust and magnetic fields. By mass, the ISM consists of about 99% gas and 1% dust, and the average particle density is one every 10^6 m^3 [4]. This may seem like a negligible amount of dust, but it can still produce serious consequences for distant objects. These dust grains do not affect the light from a star equally at all wavelengths; shorter wavelengths are preferentially scattered more than the longer wavelengths of red light. As a result, a star will appear more red to a distant observer than it really is. This effect is called interstellar reddening.

Since interstellar reddening is wavelength-dependent, it affects our traditional color indices and therefore our temperature measurements. For ground based telescopes there are also additional corrections that need to be made for atmospheric extinction. To overcome these effects, it is possible to use a variety of complicated methods including three-color (or more) photometry [5].

A more simple way to avoid interstellar reddening is to use a single wavelength index. As previously mentioned, this is achieved by using two filters of different bandwidths centered on the same wavelength. Since light is measured at a single wavelength only, all measurements are equally affected by atmospheric extinction and interstellar reddening, so no corrections are necessary.

1.5 Advantages of an Hα Index over an Hβ Index

A substantial amount of work has been performed previously using filters centered on the Hβ line (4861Å) of the Balmer series [6] [7]. There has been some work performed using an Hα index [8] [9], but currently the Hβ system is still more popular and more widely used. However, we show that there are several advantages to using an index centered on the Hα line. First, the sensitivity of a Charge-Coupled Device (CCD) is determined by its quantum efficiency (QE), which is defined as the percentage of photons hitting the photoreactive surface that activate it relative to the total number of incoming photons. A QE of 100% would be indicative of a perfect detector.

QE is always a function of wavelength, so certain wavelengths will yield a greater QE than others. When research was first being performed using the Hβ index, photomultipliers were the most common detectors. These detectors had a greater QE in the Hβ range than in the Hα range. However, CCDs are currently the most common detector and, as shown in Fig. 1.5, they approach 100% efficiency in the red region

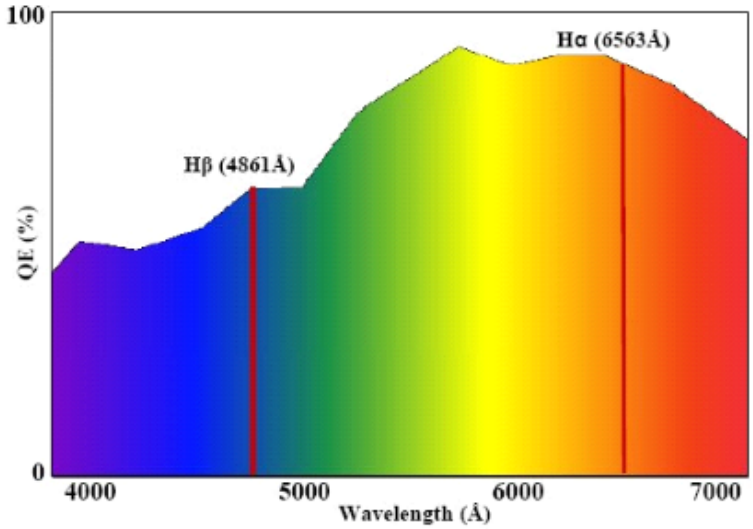

Figure 1.5: Quantum efficiency of a typical CCD showing greater sensitivity in the Hα region than the Hβ region.

of the spectrum. Since this corresponds to the wavelength of the Hα line, it is more advantageous to use an Hα index than an Hβ index. More details on detectors will be given in Sec. 2.4.

Another advantage of Hα over Hβ is that there are always fewer absorption lines in the Hα region than the Hβ region. This can be seen in Fig. 1.6 where the Hα line is much cleaner than the Hβ line, which has a lot more interference surrounding it. Thus, light passing through the Hβ wide filter is more likely to be affected by other nearby absorption lines than light passing through the Hα wide filter. This effect is known as line blanketing.

Finally, the Hα index has the capability of detecting a wider range of spectral types. Even though hot stars have a peak intensity in the Hβ region, the overall intensity is so great that it is still easy to obtain measurements in the Hα region. Cooler stars, however, have a peak intensity at red wavelengths where the Hα line

appears. For these stars, the overall intensity is so much lower that an accurate measurement in the Hβ region is no longer possible. Consequently, an Hα catalogue is able to include late G-type stars, whereas the Hβ catalogues can only go down to late F-type stars.

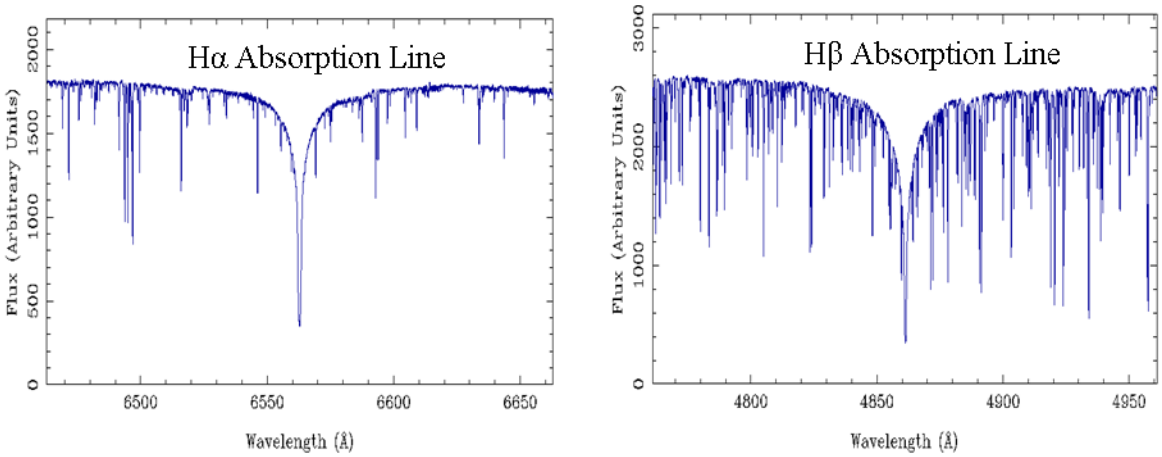

Figure 1.6: Stellar spectrum of Procyon, spectral type F5IV, showing less line blanketing around the Hα region (left) than the Hβ region (right). Adapted from http://www.sc.eso.org/santiago/uvespop/bright_stars_uptonow.html

Chapter 2

Equipment and Observations

2.1 Orson Pratt Observatory

Figure 2.1: BYU's Orson Pratt Observatory.

Most of the data for this project were obtained using the 16" David Derrick Telescope (DDT) at Brigham Young University's (BYU) Orson Pratt Observatory (OPO) (Fig. 2.1). Located in Provo, Utah, the observatory is at an elevation of 4,720 feet [10]. The DDT, shown in Fig. 2.2, was installed 26 March 1998 and is conveniently situated on the sixth floor of the Eyring Science Center (ESC). This

has the major advantage of being easily accessible to students and faculty who might otherwise have to travel long distances to obtain telescope time. It does have some distinct disadvantages though, including exhaust vents on the ESC roof, a heating plant to the east, bright lights from other buildings on campus and the city of Provo, and a twelve-story building directly to the west. However, by planning the observing program carefully, the effects from these problems can be mitigated.

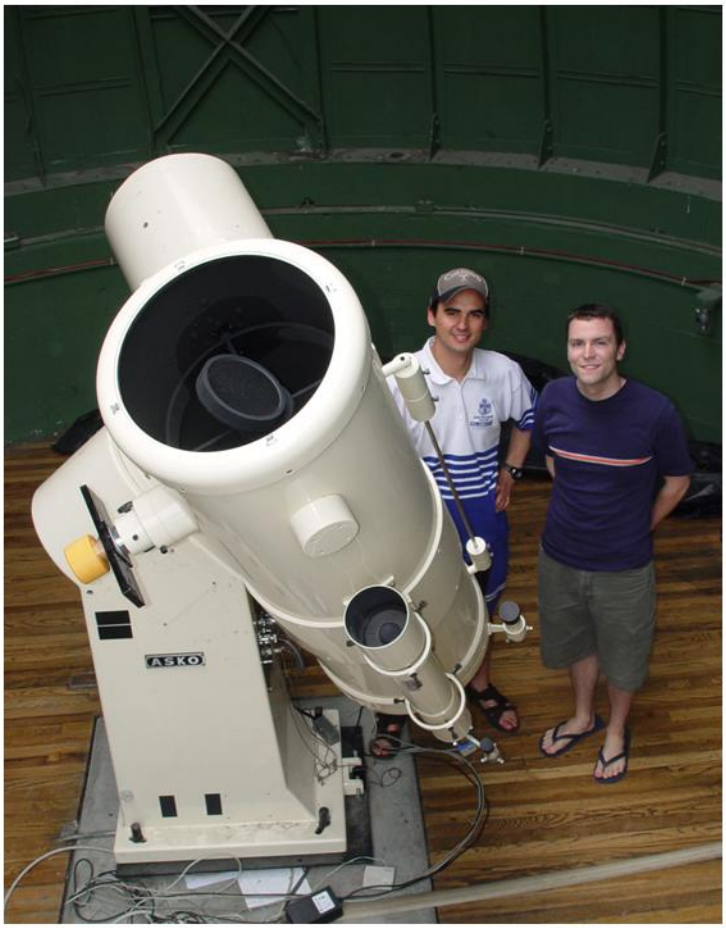

Figure 2.2: Mana Vautier and Canon Laverty standing next to BYU's 16" David Derrick Telescope.

The DDT is a dual focus telescope, which means that the secondary mirror can be rotated to focus the light to the back or the side of the telescope, providing two different possible focal lengths known respectively as Cassegrain and Newtonian foci. These focal lengths determine the plate scale. Plate scale relates the angular field of view of a frame to the size of the detector, and is generally reported in units of arcsec/mm. My research utilized the Cassegrain focus only, mounted with an ST-1001 CCD. The specifications for this particular combination are listed in Table 2.1.

Table 2.1: Specifications for telescope/CCD combinations.

	OPO **ST-1001**	WMO **ST-10**
Diameter	406 mm (16in)	203 mm (8in)
Focal Ratio	f/16	f/4
Focal Length	6496 mm (258in)	812 mm (32in)
Plate Scale	31.75"/mm	254"/mm
Pixel Size	24 μm	6.8 μm
CCD Size	24.6 x 24.6 mm^2	14.7 x 10 mm^2
Imaging Array	1024 x 1024 pixels	2184 x 1472 pixels
Field of View	13' x 13'	62.87' x 42.37'
Resolution/Pixel	0.762"	1.727"

2.2 West Mountain Observatory

Located on top of a mountain about one hour from BYU toward the south end of Utah Lake, West Mountain Observatory (WMO) is at an elevation of 6,700 feet [11]. Typically, 60 nights per year are suitable for all-sky photometry and an additional 100 nights per year can be used for differential photometric work.

The actual observatory was built in 1981 and contains several work areas, a small library, a local area network, kitchenette, lavatory, and two dorm rooms. The main dome to the south of the building has a diameter of 7 meters and a 1.3 meter wide slit. Visible just behind the main building in Fig. 2.3 is the smaller dome which houses an

8" Meade reflector mounted on a Paramount ME. Two nights of data for this project were obtained with this telescope, and the specifications are listed in Table 2.1.

Figure 2.3: BYU's West Mountain Observatory.

2.3 Filters

Filters are often used to examine various regions of a star's blackbody curve. A blackbody is an object that absorbs all the electromagnetic radiation that falls on it. Although no radiation is reflected, a certain amount of energy is radiated according to the temperature of the object. The corresponding intensity of this radiation is dependent upon wavelength. As shown in Fig. 2.4, cooler objects have a peak intensity at higher wavelengths than hotter objects. A star's blackbody curve has approximately the same shape as a perfect blackbody with the same temperature. The color index of a star (Sec. 1.2) obtained by measuring magnitudes through two filters centered on different wavelengths effectively measures the slope of the star's blackbody curve which is directly related to the temperature of the the star (Fig. 2.4).

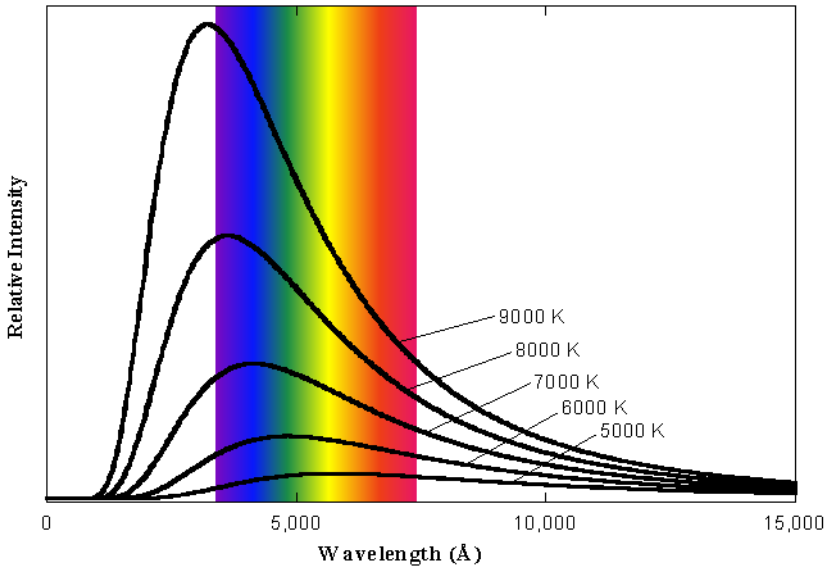

Figure 2.4: Graphical representation of blackbody curves for several different temperatures.

There have been many different filter systems designed to examine a range of spectral features with varying amounts of detail. As mentioned in Sec. 1.2, Johnson UBVRI and Strömgren *uvby* filters are two commonly used systems. The Johnson system is considered a broadband system since each filter generally has a passband about 1000Å wide. These systems cover a wide range of spectral features, but provide less detailed information on each feature. However, since the passband is fairly wide, a lot more light is allowed through and exposure times are shorter.

The Strömgren filters are known as intermediate filters with passbands on the order of 200-300Å. These filters are generally designed to give information near certain spectral regions, and are often used specifically to study a certain type of object.

A final set of filters are identified as narrow filters and range from 5-100Å in width. These filters are usually placed on or near specific spectral features such as the Hβ, S II and O III lines. As mentioned in Sec. 1.2, the filters used for this project were centered on the Hα line of the Balmer series, and had passbands of 30Å and 210Å for the narrow and wide filters, respectively. A transmission profile for each of these filters is shown in Fig. 2.5.

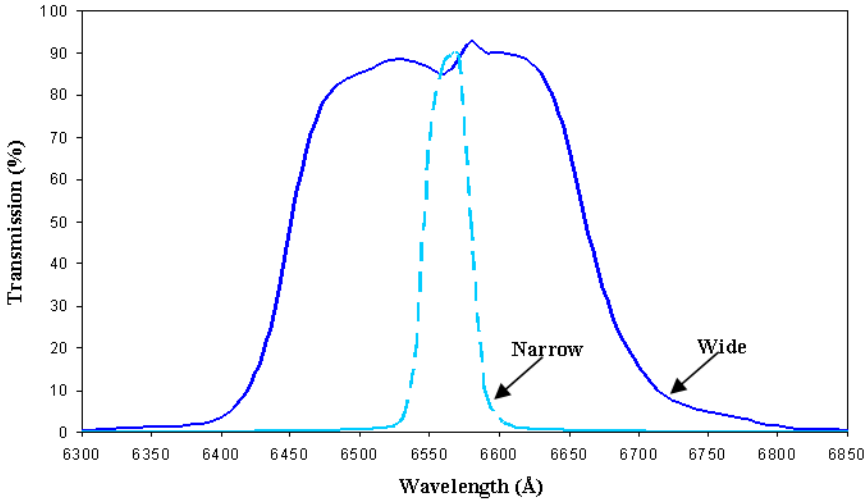

Figure 2.5: Transmission profiles of the narrow and wide Hα filters.

2.4 Charge-Coupled Devices

One of the main objectives of astronomy is to count photons in order to determine the brightness, or magnitude, of stars. This can be accomplished using various detectors including the human eye, photographic plates, photomultipliers, and CCDs. Hipparchus actually became quite talented at measuring the magnitude of stars using only his eyes, and was the first to define a stellar magnitude system. He grouped the stars into six categories, 1^{st} magnitude being the brightest and 6^{th} the faintest. It was later discovered that an object five magnitudes less than another object essentially

corresponded to being 100 times brighter, and that the human eye was somewhat logarithmic in response. Obviously this was not a very precise method, and no permanent image was produced.

The first detectors to produce a permanent image were photographic plates. These plates also improved magnitude measurements. On the downside, these detectors only have a linear response in a narrow dynamic range and collect less than 1% of the incident photons. A better alternative is the photomultiplier, or PM, which is particularly sensitive for wavelengths ranging from ultraviolet to infrared. As their name suggests, these detectors multiply the signal produced from incident light. Sensitivity is high enough to detect single photons and amplify them to measurable signals, yielding very reasonable quantum efficiency. However, two disadvantages of PMs is that only one object is observable at a time, and that photometric conditions (Sec. 3.3) are required.

Currently, the most common detector in astronomy is the CCD camera. These detectors consist of an integrated circuit containing an array of coupled "capacitors" which essentially act as photon counters. These photosensitive elements, or pixels, turn light into electrons which collect in "wells". We can then read the counts in each well and know how much light we are receiving in each pixel. CCD's have several advantages over other detectors including very high quantum efficiency, production of a permanent image, and the fact that many objects can be observed simultaneously. They also have a linear relation across the chip, which means that something twice as bright generates twice as many counts in the same amount of time. However, there are a few concerns associated with using CCDs which necessitate three calibration frames being taken as discussed in Sec. 3.1.

2.5 The Pleiades

Star clusters are groups of stars which are gravitationally bound. Two distinct types of star clusters can be distinguished. Globular clusters are tight groups of hundreds of thousands of very old stars, while open clusters generally contain a few hundred members and are often very young.

Globular clusters are roughly spherical groups of anywhere from 10^4 to 10^6 stars spanning a distance of 10^1 to 10^2 light years in diameter. They are estimated to be 12 to 16 billion years old, and contain mostly yellow and red stars which weigh less than about two solar masses. This is because the hotter, more massive stars have either exploded as supernovae or passed through a planetary nebula phase to become white dwarfs. The approximately 150 globular clusters in our Milky Way galaxy are predominantly located in the galactic halo.

Open clusters (sometimes called galactic clusters) are quite different from their globular counterparts. They are typically only 100 to 500 million years old, contain far fewer stars, and are confined to the spiral arms in the galactic plane. Although the stars within an open cluster are still gravitationally bound, the overall gravitational attraction is not as strong as globular clusters since they are much less densely populated.

The Pleiades, also known as M45 or the Seven Sisters, is an open cluster in the constellation of Taurus. At a distance of about 440 light years, it is one of the closest open clusters to the earth, probably the best known and certainly the most striking to the naked eye. Approximately 500 stars make up the cluster, most of which are young, hot blue stars about 115 million years old. A list of target stars from the Pleiades is given in Table B.2 of the Appendix, along with other stars used to standardize the system. A detailed explanation of the standardization process is given in Sec.3.4.

A total of 24 Pleiades stars were observed over seven nights between September 2005 and February 2006 using two W,N,N,W palindrome sequences, and each of these stars is shown in Fig. 2.6. All the selected stars are well studied, known members of the cluster and have a range of spectral types from B6 to G0. Although most stars are main sequence dwarfs, there are also a couple of normal giants and subgiants. A more complete list of observations by night, including Hyades stars and field stars, is shown in Table B.1 of the Appendix.

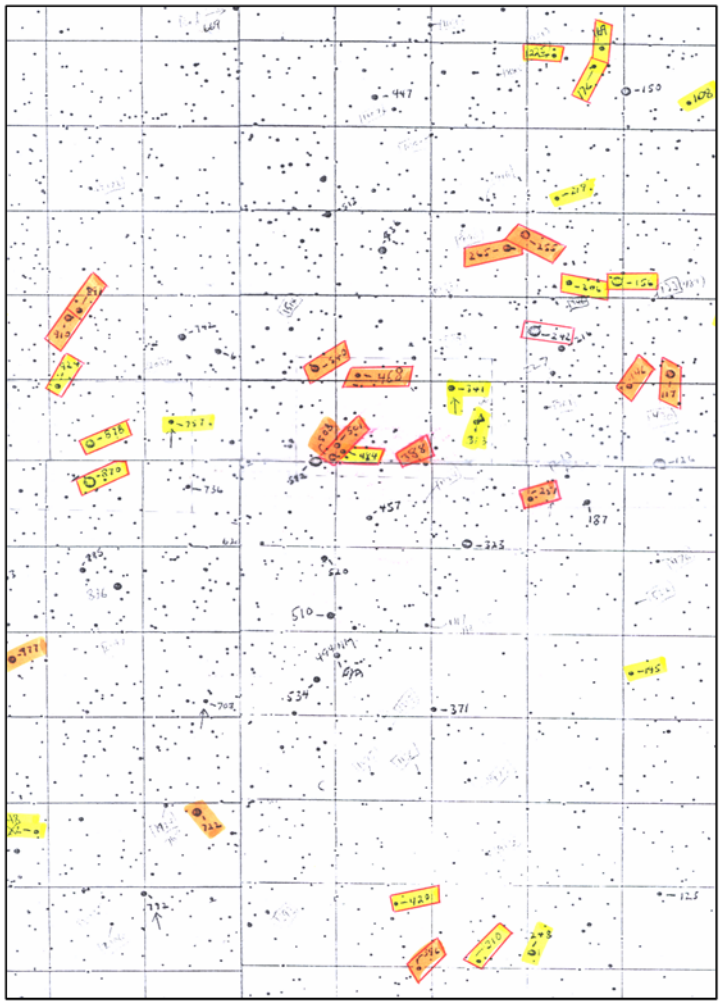

Figure 2.6: Finder chart of the Pleiades. The 24 selected stars are labeled with a red border.

Chapter 3

Reduction Methods and Data Analysis

3.1 Calibration Frames

Raw data must first be reduced to obtain high quality results for analysis. Typically three frames are required for the reduction process: bias frames, dark frames, and flat frames. The bias, or zero, frame has an integration time of zero seconds, and removes electrons which are inherently present in the wells of the CCD. These electrons are created by the electronics and amplifiers of the CCD, even when it is not exposed to light. Bias frames are averaged together, then subtracted out of the object frames.

Since CCDs are powered electronically, a current is applied to the detector causing some electrons to get into the wells independently from photon detection. This "dark" current is sensitive to temperature and proportional to exposure length. For this reason, CCDs are ideally cooled to at least -20℃ and have an integration time corresponding to that of the object frame. Since these frames are taken with the shutter closed they are called dark frames, and once again they are averaged together

and subtracted out of the object frame.

Finally, flat frames are taken to compensate for the intrinsic response differences of the pixels. Even though two pixels may be right next to each other and receive equal flux, they might record different photon counts. This variation is corrected by taking an image of a uniform, or flat, field so that the same brightness covers the entire CCD chip. One easy way to achieve this is by taking a picture of the twilight sky. These flat fields are normalized and divided through each object frame by filter. All calibration frames were applied using standard reduction techniques in the Image Reduction and Analysis Facility (IRAF).

3.2 Aperture Photometry

The simplest way to measure the magnitude of a star is called aperture photometry. In this method, a circular aperture is centered on each star of interest in the image, and the photons within the aperture are counted. Since photons from the background sky and the star are included in this area, we must subtract the sky counts from the aperture counts. This is done in IRAF's apphot package by placing an annulus around the aperture, and summing the counts within the annulus. Values used in this project are shown in Table 3.1.

Table 3.1: BYU and WMO parameters used to perform aperture photometry. Values are given in pixels.

Parameter	**OPO**	**WMO**
Aperture	10	7
Inner Radius	10	9
Outer Radius	15	12

To determine the radius of the aperture and annulus, we look at the brightness of a star's image plotted as a function of distance from the image center. This plot, called a radial profile (Fig. 3.1), is typically close to a Gaussian profile and can be defined by a maximum value and a Full Width at Half Maximum (FWHM). At one FWHM, the signal to noise ratio is usually the best, and as shown in Fig. 3.1, by three FWHM, we effectively have all the light from the star.

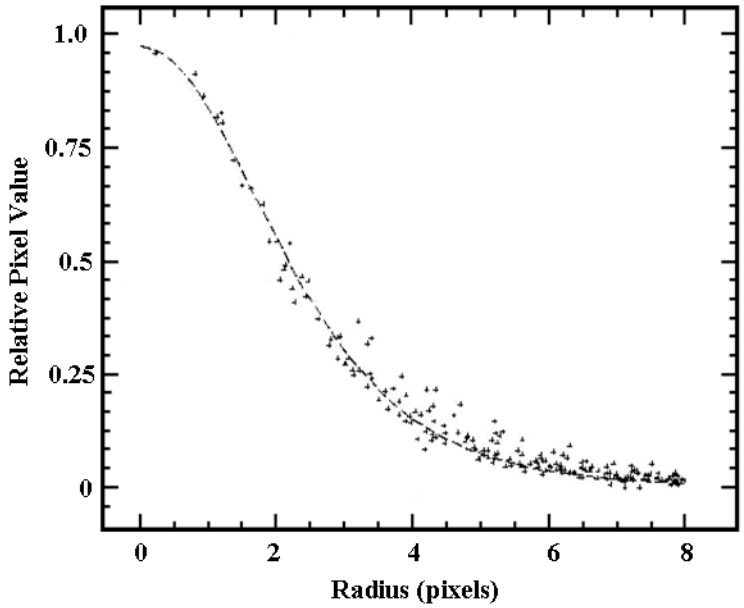

Figure 3.1: Radial Profile of Hz 206 taken from OPO showing a FWHM of approximately two.

Once IRAF has summed the counts within the annulus, the number of sky counts per pixel is determined. The sky counts are then subtracted from the aperture based on it's area to obtain the total number of counts that came from a given star over the course of an exposure. This value is divided by the length of the exposure to yield the integrated flux f in counts per second over the area of the detector. The flux can

then be converted to a magnitude using Eq. 3.1, where m is an instrumental apparent magnitude and ZP is a zero point value. A ZP value of 20 was used in performing aperture photometry on the data.

$$m = -2.5 \log_{10} f + ZP \tag{3.1}$$

3.3 Correcting the Data

The instrumental magnitudes acquired from IRAF were obtained under differing conditions, and the data needed to be standardized to bring all nights onto the "same system". These differences include observations being made at different times of year, which meant a large difference in ambient temperature. Different CCD/telescope combinations were also used between BYU and WMO observatories, although the filter set was transported between observatories so the same filters were used for all observations.

Before standardizing the data sets, corrections needed to be made to each individual sequence to eliminate possible spurious points. The most significant elimination applied was a result of non-photometric observing conditions. A night is considered to be photometric when every part of the sky is like any other part. This means there are no clouds, including light cirrus, except perhaps on the distant horizon. Even a full moon can make a night non-photometric due to an excess of light in the region of sky surrounding the moon. Sometimes conditions can be deceptive, and a night that appears photometric can produce non-photometric results. Unfortunately this was the case on December 8^{th}, 2005. After reducing the data, it was evident that the whole night had to be thrown out due to non-photometric conditions, likely caused by light cirrus.

Another correction was made due to a difference in ambient temperature during a series of sequences. Since the DDT must be moved manually, it is necessary to go into the dome each time the telescope needs to be moved. During cold weather, warm air from the building is allowed into the dome, causing the stars on the image to spill light out of them and increase in size. As a result, the stars appear fainter and the calculated magnitude is larger than expected. This is clearly seen in Table 3.2. It is evident that the first two readings of each sequence are approximately one-tenth of a magnitude greater than subsequent measurements, thus requiring they be eliminated.

Table 3.2: Data corrections due to ambient temperature gradient: 11 February 2006. Italicized values represent erroneous magnitudes.

Hz	Filter	Magnitude	**Hz**	Filter	Magnitude
255	W	*8.214*	206	W	*10.850*
255	N	*10.456*	206	N	*13.038*
255	N	10.364	206	N	12.949
255	W	8.123	206	W	10.753
255	W	8.164	206	W	10.753
255	N	10.367	206	N	12.925
255	N	10.360	206	N	12.921
255	W	8.135	206	W	10.747

Table 3.3: Data corrections due to filter slide not changing: 15 September 2005. Italicized values represent erroneous magnitudes.

Hz	Filter	Magnitude	**Hz**	Filter	Magnitude
206	W	10.642	265	W	8.868
206	N	12.803	265	N	10.957
206	N	12.797	265	N	10.995
206	W	*12.827*	265	W	*10.968*
206	W	*12.831*	265	W	*10.969*
206	N	12.839	265	N	10.977
206	N	12.823	265	N	11.000
206	W	10.651	265	W	8.831

When exposing a sequence, the filter slide should automatically switch filters. Table 3.3 illustrates an example from 15 September 2005 when this was clearly not the case. The italicized magnitudes were supposedly taken through the wide filter, but their similarity to the narrow values indicates that the filter slide never moved. All data points exhibiting this trend were identified and eliminated.

The final correction made was due to a problem with the telescope not tracking properly. When looking at some of the frames, a double image was observed such as in Fig. 3.2. All the stars in the frame look as though they have been shifted to the right. This was caused by a jump in the tracking during the exposure, and any frames with this double image characteristic were also eliminated.

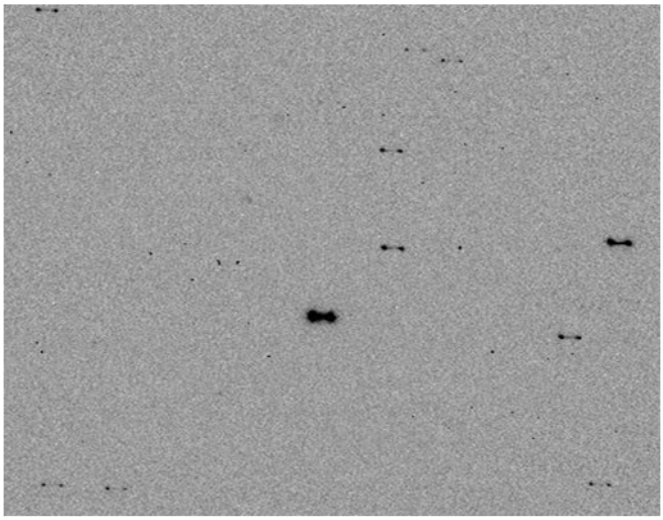

Figure 3.2: Double image caused by a jump in the telescope tracking.

3.4 Standardizing the Data

After all the data sets had been examined and corrected, each night needed to be standardized to bring them all onto the same system. The standardization process involved three main steps. First, a zero point for the Hα system had to be decided upon. Second, every other night needed to be standardized to this system. Third, the standardized data sets were checked to confirm they were all on the same system.

It is arbitrary which nights are chosen to represent the standard values, but there are two guidelines which should be observed when making the choice. First, multiple nights over a time frame of no more than a couple of weeks should be used. Second, there must be ample overlap from night to night of the stars observed. Based on these conditions, observations of the field stars from all nights in July 2005 were chosen to be the standard system.

The indices for each star from these nights were then averaged together to obtain a mean vector. Next, each index in the mean vector was subtracted from corresponding indices on all remaining nights to produce a difference vector for each night. A zero point correction for each night was then determined by calculating the average of each corresponding difference vector. Once calculated, these zero point values were applied to corresponding data sets to obtain final indices for each night.

Throughout the standardization process, Student's t-test was used extensively to confirm that all data sets were on the same system. Student's t-test, sometimes called a t-statistic or t-distribution, compares a pair of data sets to determine if any deviation between the means is within acceptable limits. For this project, the null hypothesis was not rejected unless the t-test yielded values of at least 1.96. A more detailed explanation of this distribution is given in Appendix A

3.5 Analyzing the Data

One of the significant benefits of a standard star catalogue is the ability to detect unusual stars. Looking at the plot of Hα vs $b-y$ shown in Fig. 3.3, we can immediately see that there are three field stars and one Pleiades star that lie beneath the expected curve. The name of each star is shown in the figure, and corresponding spectral types are listed in Table B.2. These wayward points are most likely the result of two effects: reddening and emission.

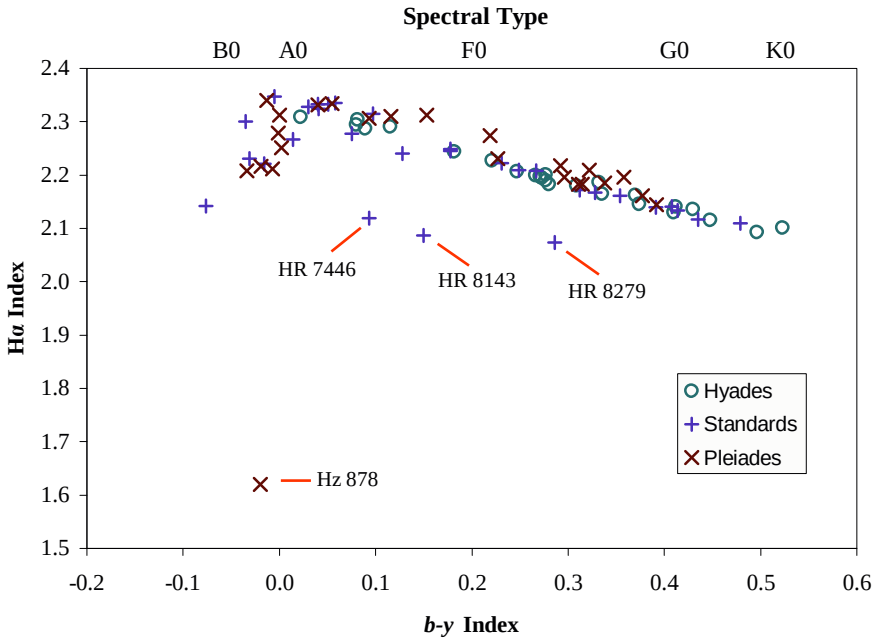

Figure 3.3: Plot comparing Hα vs $b-y$ indices for the Pleiades, Hyades and field stars.

With the exception of the three wayward stars, all of which are B-type stars, the field star data points are bound to the curve in a tight fit. This is probably due to the fact that most of the field stars are not surrounded by regions of gas and dust. The Pleiades, however, contain a lot more dust and many of the stars are reddened. Many of these stars are shifted to the right of where they should be on the plot, although

they are not shifted as much as the three field stars which are shifted by as much as three tenths of a magnitude. The reason why these stars are shifted is because the $b-y$ index is sensitive to the effects of reddening, causing a greater index value. In contrast, the Hα index remains the same since a single wavelength index is not affected by reddening.

Another observation that can be made from the $b-y$ plot is found at the peak of the curve. The strongest Hα absorption lines occur in early A-type stars. These stars typically have a $b-y$ index of close to zero, and this is what we observe on the plot. By referring to Table 4.1, we can see that the stars with the highest Hα indices have a $b-y$ index of approximately zero and, as expected, these values correspond to early A-type stars.

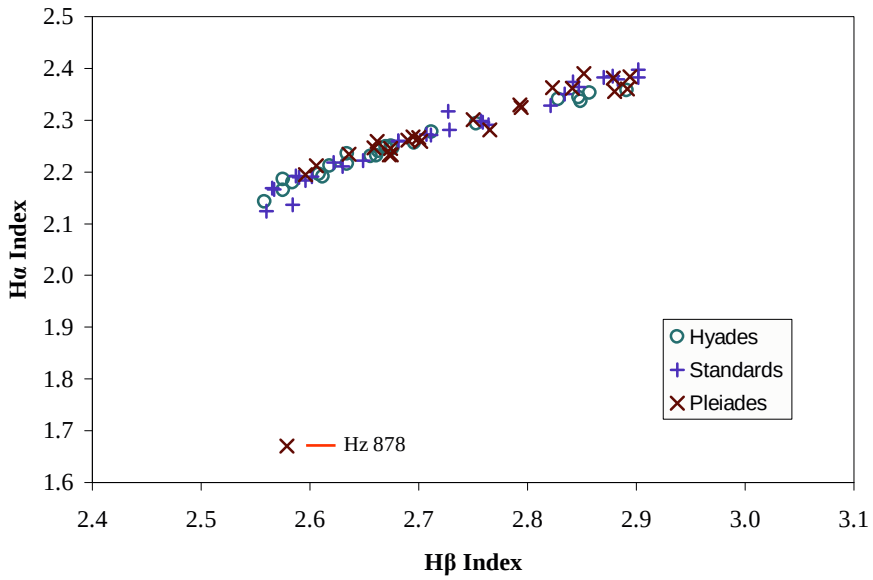

Figure 3.4: Plot comparing Hα vs Hβ indices for the Pleiades, Hyades and field stars.

A plot of Hα vs Hβ is shown in Fig. 3.4. Toward the bottom of this plot is an anomalous point with an unusually low Hα index. This point corresponds to star Hz 878, and Table 4.1 indicates that this star is actually an emission star. This is as expected for a star with a low index, because the Hα absorption line is filled by the emission features. Although it has not been affected quite as much, it is likely that B9 star HR 8143 has also been shifted in Fig. 3.3 from the presence of emission at Hα.

Fig. 3.4 also illustrates how single wavelength indices are not sensitive to the effects of reddening. Even though the same stars are used in this plot as in Fig. 3.3, the two hydrogen indices produce a linear relationship. This is as expected since hydrogen lines vary proportionally with temperature. Since emission stars affect the strength of the absorption lines, Hz 878 still appears at the bottom of the plot.

Chapter 4

Results and Conclusion

4.1 Final Indices

A final list of Hα indices for selected stars in the Pleiades is given in Table 4.1. Values for the Hβ and $b-y$ indices were taken from Crawford and Perry 1976 [12], and spectral types were obtained from the SIMBAD astronomical database [13]. The standard deviation σ was calculated using an error per observation method

$$\sigma = \sqrt{\frac{\sum_{i=1}^{n}(x_i - \bar{x})^2}{(n-1)}} \tag{4.1}$$

where x_i corresponds to each individual data point, $\bar{x}$ is the mean value of the set, and n is the total number of data points in the set.

As can be seen, observed stars cover a wide range of spectral types from late B-type stars to early G stars. Although the luminosity classes are mostly main sequence dwarfs, there are a few giants and subgiants.

Table 4.1: Final calculated Hα indices for the Pleiades and other information.

Hz	type	α	β^a	$b-y^a$	n	σ
117	B7IV	2.251	2.750	0.002	2	0.007
146	Am	2.275	2.794	0.219	2	0.006
156	B6IV	2.208	2.702	-0.034	5	0.013
169	F3V	2.218	2.695	0.292	5	0.010
176	F5V	2.185	2.636	0.338	5	0.006
206	A9V	2.231	2.765	0.227	7	0.015
225	G0V	2.144	2.596	0.392	4	0.005
242	B8III	2.212	2.690	-0.007	3	0.007
251	A2V	2.310	2.892	0.116	2	0.004
255	B8V	2.279	2.793	-0.001	7	0.022
265	A0Vn	2.313	2.823	0.000	3	0.012
310	G0V	2.161	2.606	0.377	2	0.009
388	F4V	2.182	2.675	0.311	5	0.013
396	F5V	2.182	2.673	0.315	2	0.021
420	F5	2.196	2.659	0.358	2	0.023
468	F6V	2.209	2.662	0.322	3	0.018
484	F3V	2.196	2.674	0.296	5	0.022
501	A7V	2.312	2.841	0.153	4	0.020
540	A0V	2.331	2.879	0.040	4	0.015
870	B8III	2.217	2.700	-0.019	3	0.006
878	B8IVevar	1.620	2.579	-0.020	3	0.062
891	A2V	2.334	2.894	0.055	2	0.011
910	B9.5V	2.339	2.852	-0.013	2	0.014
924	A3V	2.306	2.880	0.093	2	0.006

[a]Crawford and Perry 1976[12]

Table 4.2: Final corrected Hα indices for selected stars in the Pleiades by night.

Hz	15 Sep 05	01 Oct 05	07 Oct 05	23 Oct 05	21 Nov 05	11 Feb 06	12 Feb 06
117	—	2.256	2.246	—	—	—	—
146	—	2.270	2.279	—	—	—	—
156	2.203	—	2.223	2.210	2.217	—	2.190
169	2.230	—	—	2.219	2.204	2.222	2.216
176	2.189	—	—	2.178	2.178	2.189	2.191
206	2.253	2.244	2.209	2.236	2.233	2.218	2.226
225	—	—	—	2.142	2.150	2.147	2.139
242	2.204	—	2.218	—	2.213	—	—
251	—	2.312	2.307	—	—	—	—
255	2.307	2.310	2.286	2.259	2.271	2.261	2.263
265	2.326	2.308	2.304	—	—	—	—
310	—	—	2.168	2.155	—	—	—
388	2.160	2.193	2.184	2.191	2.184	—	—
396	—	—	2.197	2.168	—	—	—
420	—	—	2.180	2.213	—	—	—
468	—	2.190	2.213	2.225	—	—	—
484	2.168	2.217	2.190	2.218	2.185	—	—
501	2.332	2.301	2.290	—	2.325	—	—
540	2.331	2.326	2.317	2.352	—	—	—
870	—	—	2.210	2.218	2.223	—	—
878	—	—	1.691	1.577	1.594	—	—
891	—	—	2.326	2.342	—	—	—
910	—	—	2.330	2.349	—	—	—
924	—	—	2.310	2.302	—	—	—

4.2 Conclusions and Future Directions

It is an extremely long and difficult process to prepare a new standardized catalogue. Although the data obtained for this project is just a portion of what is needed for a comprehensive Hα catalogue, it comprises a large and accurate data set.

It has been shown that the Hα index has several advantages over the Hβ index, including the use of greater CCD quantum efficiency, less line blanketing in the red portion of the spectrum, and the capability to detect a wider range of spectral types. The ability to obtain a reddening free index has also clearly established the advantage of a single wavelength index.

One important procedural note made during the course of this project is the effect of temperature on the observing process. After moving the telescope, it is recommended that the next sequence not be started for approximately two minutes to allow the dome temperature to return to the ambient temperature. Ideally, there should be one person who stays up in the dome to move the telescope between sequences without having to open the trap door. This has the obvious advantage that more stars are able to be observed in a shorter amount of time, and the need for temperature corrections is eliminated.

This project has established that the Hα catalogue presented here is able to distinguish spectral types. Since spectral types are directly related to stellar temperatures, it is also possible to obtain an accurate temperature standardization from the catalogue. A comprehensive set of data has been secured for the Pleiades and, when combined with more data from other clusters, can be used to produce a very accurate and useful Hα catalogue which can be made available for use by other astronomers in their own research.

Bibliography

[1] M. S. Bessell, "UBVRI photometry. II - The Cousins VRI system, its temperature and absolute flux calibration, and relevance for two-dimensional photometry," PASP **91,** 589–607 (1979).

[2] J. D. Fernie, "Relationships between the Johnson and Kron-Cousins VRI photometric systems," PASP **95,** 5782–785 (1983).

[3] D. L. Crawford and J. V. Barnes, "Standard Stars for uvby Photometry," AJ **75,** 978–998 (1970).

[4] *Introductory Astronomy and Astrophysics*, 4th ed. (Saunders College Publishing, Fort Worth, TX, 1998).

[5] L. N. Knyazeva and A. V. Kharitonov, "Observed and Calculated Normal Color Indices and Indices in Three Photometric Systems," Astronomy Reports **46,** 152–160 (2002).

[6] D. Crawford and J. Mander, "Standard Stars for Photoelectric $H\beta$ Photometry," AJ **71,** 114–118 (1965).

[7] D. Crawford and J. Mander, "Early-Type Stars Used as Standards in Photoelectric Hβ Photometry," ApJ **132,** 66–67 (1960).

[8] D. W. Peat, "Hα Photometry of late-type stars I. F, G and K-type stars north of the equator," MNRAS **128,** 435–473 (1964).

[9] J. Dachs and T. Schmidt-Kaler, "Standard Stars for Photoelectric $H\alpha$ Line Photometry," A&AS **21,** 81–97 (1974).

[10] B. Peterson, "BYU Weather Station," http://marvin.byu.edu/Weather/AboutStation.htm pp. [Online; accessed 25–April–2006] (2006).

[11] I. Maps a la carte, "TopoZone," http://www.topozone.com/map.asp?lat=40.08889&lon=-111.82139 pp. [Online; accessed 25–April–2006] (2006).

[12] D. Crawford and C. L. Perry, "Four Color and $H\beta$ Photometry of Open Clusters. XI. The Pleiades," AJ **81,** 419–426 (1976).

[13] SIMBAD, "SIMBAD Astronomical Database," http://simbad.harvard.edu/cgibin/WSimbad.pl pp. [Online; accessed 23–March–2006] (2006).

[14] Wikipedia, "Student's t-test — Wikipedia, The Free Encyclopedia," http://en.wikipedia.org/w/index.php?title=Studentpp. [Online; accessed 23–March–2006] (2006).

Appendix A

Student's *t* test

Student's t-test was used to confirm that all data sets had been standardized properly. This statistic was developed by William Gosset in 1908, and was first published in "Biometrika" that same year under the pen name "Student" [14]. Gosset worked at the Guinness brewery in Dublin, Ireland and formulated the t-test to ensure that all batches of whisky were as similar as possible.

To perform the t-test, a difference vector was first obtained for any two nights of interest and an average value $\bar{x}$ for that vector was calculated. A standard deviation σ_m for the same difference vector was then determined using an error per mean method as shown in Eq. A.1, where x_i corresponds to each individual data point, x is the mean value of the vector, and n is the total number of data points in the vector.

$$\sigma_m = \sqrt{\frac{\sum_{i=1}^{n}(x_i - \bar{x})^2}{n(n-1)}} \tag{A.1}$$

A final value of t is obtained by dividing the average value by the standard deviation. The threshold value of 1.96 for a 95% confidence interval used for this project was acquired from a standard t-test table.

Appendix B

Observations

The tables below provide more specific information about observations, including information on the Hyades and field stars. Table B.1 lists the number of stars observed in each field by date. Italicized dates indicate data obtained at WMO. All observed Pleiades, Hyades and field stars are listed in Table B.2 with their corresponding spectral type and luminosity class.

Table B.1: Observations by date.

Date	The Pleiades	The Hyades	Field Stars
02 Jul	—	—	9
12 Jul	—	—	11
19 Jul	—	—	17
02 Sep	—	—	11
15 Sep	14	—	15
01 Oct	13	—	—
07 Oct	24	—	8
22 Oct	—	—	—
03 Oct	22	25	8
21 Nov	15	24	19
11 Feb	5	14	2
12 Feb	6	21	2

Table B.2: Selected target stars.

The Pleiades		**The Hyades**		**Field Stars**	
star	type	star	type	star	type
Hz 117	B7IV	vB 6	F4V	HD 161817	A2VI
Hz 146	Am	vB 7	K2	HR 0063	A2V
Hz 156	B6IV	vB 10	G0	HR 0068	A2V
Hz 169	F3V	vB 13	F6V	HR 5062	A5V
Hz 176	F5V	vB 16	F5V	HR 5447	F2V
Hz 206	A9V	vB 17	G5	HR 5936	F0IV
Hz 225	G0V	vB 18	G0	HR 5968	G2V
Hz 242	B8III	vB 19	F8V	HR 6355	A4IV
Hz 251	A2V	vB 27	G8V	HR 7178	B9III
Hz 255	B8V	vB 35	F5V	HR 7235	A0Vn
Hz 265	A0Vn	vB 37	F5V	HR 7253	F0III
Hz 310	G0V	vB 46	G5	HR 7446	B0III
Hz 388	F4V	vB 47	A7V	HR 7447	B5III
Hz 396	F5V	vB 48	F8V	HR 7462	K0V
Hz 420	F5	vB 53	F4V	HR 7469	K4V
Hz 468	F6V	vB 56	A2IV	HR 7503	G1V
Hz 484	F3V	vB 64	G2V	HR 7504	G2V
Hz 501	A7V	vB 74	A7V	HR 7534	F7V
Hz 540	A0V	vB 86	F5V	HR 7560	F8V
Hz 870	B8III	vB 90	F5V	HR 7610	A1IV
Hz 878	B8IVevar	vB 94	F2	HR 8143	B9Ia
Hz 891	A2V	vB 108	A5Vn	HR 8279	B2Ib
Hz 910	B9.5V	vB 118	F8V	HR 8494	F0IV
Hz 924	A3V	vB 126	F3IV	HR 8622	O9V
—	—	vB 129	A7V	HR 8826	A5V
—	—	—	—	HR 8965	B8V
—	—	—	—	HR 8969	F7V
—	—	—	—	HR 8976	B9IV
—	—	—	—	HR 9088	G2V
—	—	—	—	HR 4738	A4V

Appendix C

AAS Poster

The following poster was presented in January 2006 at 207$^{\text{th}}$ American Astronomical Society Meeting in Washington D.C.

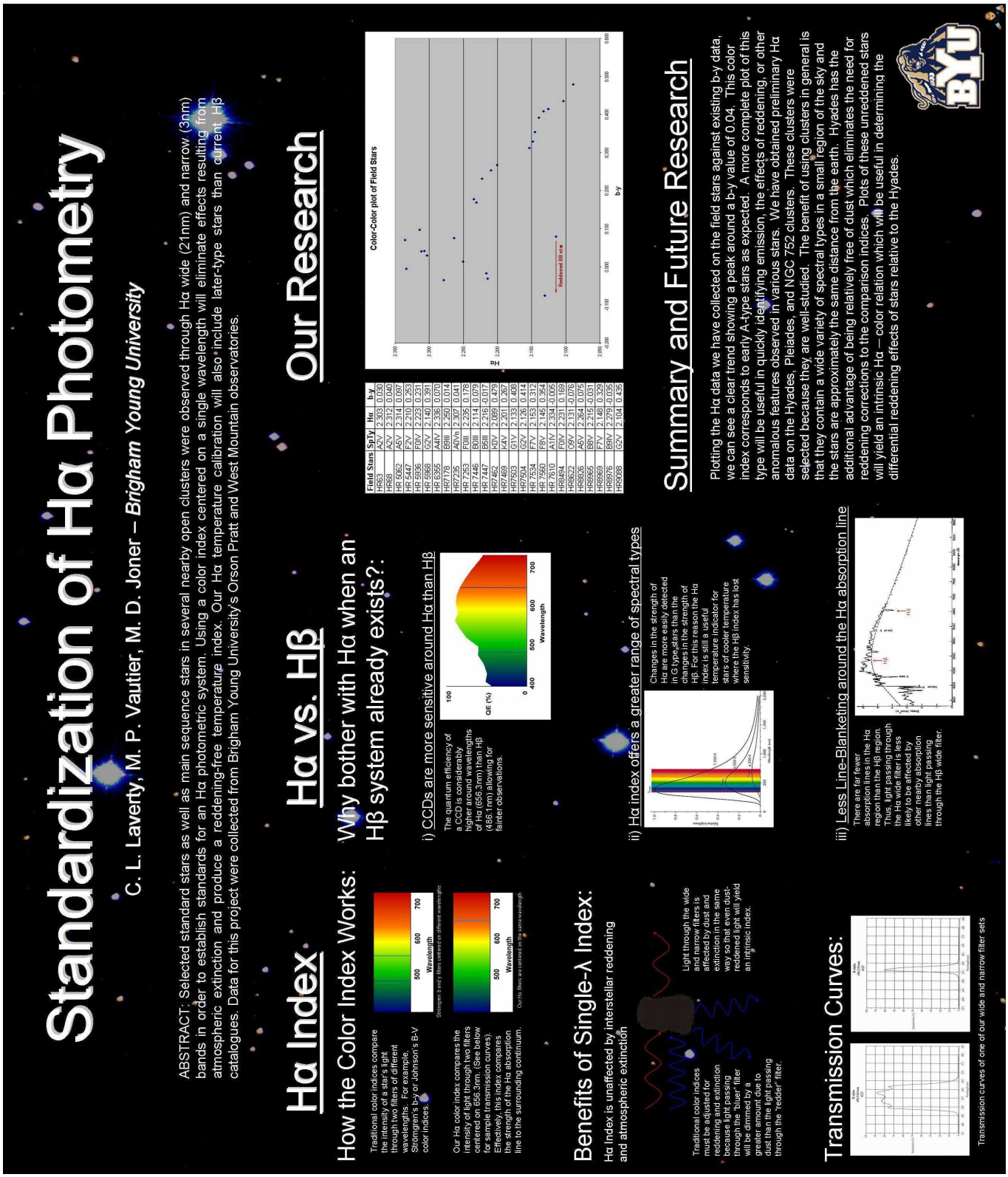

Figure C.1: AAS Poster

Index